

Vibrations of free and embedded anisotropic elastic spheres: Application to low-frequency Raman scattering of silicon nanoparticles in silica

Lucien Saviot,¹ Daniel B. Murray,² and Maria del Carmen Marco de Lucas¹

¹*Laboratoire de Recherche sur la Réactivité des Solides, UMR 5613 CNRS - Université de Bourgogne
9 avenue A. Savary, BP 47870 - 21078 Dijon - France**

²*Department of Physics, Okanagan University College, Kelowna, British Columbia, Canada V1V 1V7†
(Dated: June 11, 2018)*

Vibrational mode frequencies and damping are calculated for an elastic sphere embedded in an infinite, homogeneous, isotropic elastic medium. Anisotropic elasticity of the sphere significantly shifts the frequencies in comparison to simplified calculations that assume isotropy. New low frequency Raman light scattering data are presented for silicon spheres grown in a SiO₂ glass matrix. Principal features of the Raman spectrum are not correctly described by a simple model of the nanoparticle as a free, isotropic sphere, but require both matrix effects and the anisotropy of the silicon to be taken into account. Libration, not vibration, is the dominant mechanism.

PACS numbers: 63.22.+m, 78.30.-j, 43.20.+g, 02.70.Ns

I. INTRODUCTION

The classical continuum mechanical problem of the vibrational frequencies of a homogeneous, isotropic, free sphere was solved exactly long ago in terms of roots of spherical Bessel functions¹. It finds application in seismology², foam spheres³ and even kidney stones⁴. Progress has also been made on generalizations of this problem. Closed form solutions are obtainable for special cases of inhomogeneity with certain special kinds of anisotropy⁵, and isotropy with radial inhomogeneity⁶. Generalized anisotropy can be handled for a sphere and other shapes with a basis function expansion⁷.

Application of the Lamb solution to metal or semiconductor spheres a few nanometers in size has been successful in explaining vibrational frequencies observable using low frequency Raman light scattering⁸ and other methods⁹. These "nanoparticles" are not truly free, but are embedded inside a glass matrix and frequently are nearly spherical. The Lamb solution is useful because of the sharp change of acoustic impedance $z = \rho c$ at the nanoparticle-glass boundary as long as the nanoparticle is much heavier or much harder than the glass. The applicability of this is challenged in the case of silicon nanoparticles grown in SiO₂ glass, where the densities are almost the same and the speed of sound in silicon is only 1.5 times faster than in glass. Also, silicon is far from isotropic with Zener anisotropy factor 1.6.

The nanoparticle's vibrational frequencies become complex valued due to damping of the modes as energy is mechanically radiated away from the nanoparticle into the surrounding glass matrix¹⁰. The effect of coupling the nanoparticle to the matrix is to shift the frequencies of the modes and dampen them¹¹. Some qualitatively new vibrational modes appear even in the limit of weak coupling¹². The solution to the elastic mechanical problem of an elastically anisotropic sphere embedded in an infinite elastic continuum has not been presented before. Here we employ both a closed form solution for the case of

isotropic elasticity as well as molecular dynamics (MD) simulations for the case of a cubic crystal with elastic constants C_{11} , C_{12} and C_{44} . The agreement of these two methods for the exactly solved free sphere case allow us to be confident in the correctness of our solution. Two different computer programs were written for the embedded isotropic sphere calculation. These cross checks are essential to avoid errors that have occurred elsewhere in the literature of this subject.

II. THEORY

The displacement field $\vec{u}(\vec{r}, t)$ of an elastic medium of density $\rho(\vec{r})$ is governed by Navier's equation: (1).

$$c_{ijkl,j}u_{k,l} + c_{ijkl}u_{k,lj} = \rho\ddot{u}_i \quad (1)$$

where $c_{ijkl}(\vec{r})$ is the 4th rank elastic tensor field with 21 independent components. In a homogeneous, isotropic medium, Eq. 1 takes the form of Eq. 2 where λ and μ are Lamé's constants.

$$(\lambda + 2\mu)\vec{\nabla}(\vec{\nabla} \cdot \vec{u}) - \mu\vec{\nabla} \times (\vec{\nabla} \times \vec{u}) = \rho\ddot{\vec{u}} \quad (2)$$

To elucidate the key features and physical basis of the motion, the vibrations of the nanoparticle are calculated here using three methods: (A) analytic solution of a free isotropic sphere reprising reference¹; (B) analytic solution of an isotropic sphere embedded in an infinite matrix; (C) MD computer simulation of a free sphere including anisotropy. Method (B) has previously been used only for some spheroidal modes^{9,13} or limiting cases¹⁰. Method (C) is reported for the first time.

The following comments apply to methods (A) and (B) which are able to exploit spherical symmetry. The time dependence of the displacement is taken as $\vec{u}(\vec{r}, t) = \vec{u}(\vec{r})e^{i\omega t}$, where ω can be complex. The angular frequency ω (in rad/s) is related to wavenumber ν (in cm⁻¹) through $\nu = \omega/(200\pi c)$, where c is the speed of light (in

m/s). In what follows, all of the results are reported in terms of $Re(\nu)$ (energy) and $Im(\nu)$ (damping).

To solve Eq. 2, a scalar and a vector potential are introduced which correspond to dilatational and equivoluminal motions respectively. Eq. 2 separates into scalar and vector parts. Detailed expressions for the displacement \vec{u} and the stress tensor $\vec{\sigma}$ can be found in¹⁴. In a previous work⁶, we expressed \vec{u} and $\vec{\sigma} \cdot \vec{r}$ in a more convenient basis. Next, boundary conditions corresponding to the system have to be applied and result in secular equations whose complex valued roots gives the frequencies of the eigenmodes of vibration. Within the nanoparticle, the scalar and vector potentials involve the spherical Bessel function of the first kind j_l .

For method (A) there is no external force on the sphere so that $\vec{\sigma} \cdot \vec{r} = \vec{0}$ at every point on the surface. For method (B), the continuity of \vec{u} and $\vec{\sigma} \cdot \vec{r}$ is imposed at the surface of the nanoparticle where it contacts the matrix.

If the glass matrix is a free sphere of radius R_m concentric around the nanoparticle of radius R_p , normal mode frequencies can be found⁶. But what happens is that every eigenfrequency vanishes as R_m^{-1} as $R_m \rightarrow \infty$. In other words, for a macroscopic glass matrix there is a continuum of states but no discrete modes.

The approach of method (B) is to look for damped modes of vibration of the nanoparticle where ω is now a complex number such that $Re(\omega)$ is the frequency of the vibration and $Im(\omega)$ is the damping. In the glass matrix, the spherical Hankel function of the second kind, $h_l^{(2)}(kr)$, is used because it corresponds to an outward travelling wave. The wavevector k is also complex.

Equations for the embedded sphere case of method (B) have already been written by Dubrovskiy et al.¹⁰. In order to find the roots of the secular equation, Dubrovskiy et al. made approximations which depend on the relative values of the parameters in the sphere and around it. We made no approximations and found the complex roots numerically²². Frequencies and damping in¹³ were reproduced with this method.

Method (C) is a molecular dynamics calculation¹⁵. While this approach can readily be extended to the more general case of an object of arbitrary shape with inhomogeneous anisotropic elasticity, we choose for brevity only to present the case of a spherical object with cubic crystalline elasticity. A simple cubic $a \times a \times a$ lattice of N identical point particles of mass ρa^3 interacting through "springs" has particle positions \vec{r}_j integrated in time and Fourier transformed in order to obtain mode frequencies. Each particle has six first neighbors and twelve second neighbors. Every pair (i, j) of first neighbors are coupled by potential energy $\frac{1}{2}k_{sp1}(\|\vec{r}_i - \vec{r}_j\| - a)^2$, while second neighbor pairs (i, j) are coupled by $\frac{1}{2}k_{sp2}(\|\vec{r}_i - \vec{r}_j\| - \sqrt{2}a)^2$. Cubic octets are coupled by $(k_{sp2}/4a^2)(D - 6a^2)^2$ where $D = \sum_{j=1}^8 \|\vec{R}_{cm} - \vec{r}_j\|^2$ and $\vec{R}_{cm} = \frac{1}{8} \sum_{j=1}^8 \vec{r}_j$. The bulk modulus is $B = (C_{11} + 2C_{12})/3$. A small isotropic dilatation $\delta = dV/V$ stretches all neighbor distances proportionally and leads to stored energy $\frac{1}{2}VB\delta^2$,

so that we obtain $a(C_{11} + 2C_{12}) = k_{sp1} + 4k_{sp2} + 24k_{sp2}$. Considering that a transverse plane wave moves along the x-axis at speed $\sqrt{C_{44}/\rho}$, we find $aC_{44} = k_{sp2}$. Finally, considering that a longitudinal plane wave moves along the x-axis at speed $\sqrt{C_{11}/\rho}$, we find $aC_{11} = k_{sp1} + 2k_{sp2} + 8k_{sp2}$. Inversion allows the three force constants to be obtained for a general cubically elastic material: $k_{sp1} = a(C_{11} - (C_{12} + C_{44}))$, $k_{sp2} = aC_{44}$ and $k_{sp2} = \frac{1}{8}a(C_{12} - C_{44})$.

The frequency dependence of a given mode is $f(N)$. A sequence of simulations with N varying from a few hundred to 210000 is used to extrapolate $f(\infty)$, which is the continuum limit. Accurate results are obtainable with just a few thousand. Actual nanoparticles are not continuum objects, and so the continuum limit is an idealization. Furthermore, our calculation uses the bulk elastic coefficients of silicon. Surface effects (arguably, the entire bulk of the nanoparticle is close to its surface) and dispersion (effects of the silicon crystal structure on phonon speed) are not taken into account in this calculation. However, the wavelengths of the lowest modes are so large compared to interatomic distances that dispersion will be negligible.

The correctness and degree of convergence of method (C) was checked by comparing its results to those of method (A) for isotropic elastic materials of various Poisson ratios. The results of the two methods agree closely.

Since the first report of low-frequency Raman scattering from nanoparticles⁸, such measurements have been made on many materials²³. Results are most often successfully explained with the free sphere model described above. However, calculated frequencies are much too high in silicon nanoparticles embedded in a silica matrix^{16,17}. In this work, we want to see if the situation can be improved by taking into account the presence of the matrix and the elastic anisotropy of silicon.

III. EXPERIMENT

New experimental results using the samples studied in¹⁷ have been obtained. The experimental setup is a Jobin-Yvon T64000. Incident light comes from the 514.5 nm line of an Argon ion laser and is focused onto a $1 \mu\text{m}^2$ area on the sample. Power was kept below 1 mW to avoid sample heating. The CCD detector allows for long accumulation times; the quality of the spectra is much improved compared to previous measurements using a scanning monochromator coupled with a photomultiplier. Spectra obtained for the sample heat treated at 500 °C are presented in Fig. 1. Measurements were made with the sample at room temperature. Average nanoparticle diameter measured by transmission electron microscopy is 6.8 nm. The two narrow lines centered around 23 and 29 cm^{-1} are plasma lines from the laser. The parallel and crossed spectra correspond to scattered light intensity with polarization parallel (I_{\parallel}) and perpendicular (I_{\perp}) to the excitation beam respectively.

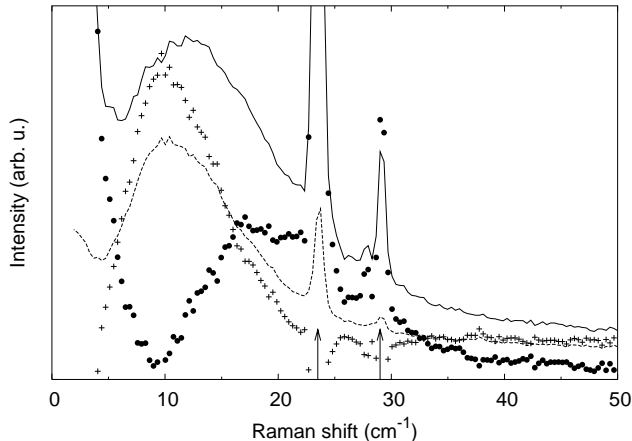


FIG. 1: Parallel (solid line) and crossed (broken line) configuration Raman spectra of 6.8 nm diameter silicon nanoparticles embedded in silica. A decomposition is made into peaks with depolarization factor 0.75 (plus signs) and 0.33 (bullets). Laser plasma lines are indicated by arrows.

The positions of the peak maxima of these two spectra differ slightly indicating scattering by several vibrational modes, one being strongly depolarized at low frequency and another less depolarized contribution at higher frequency. From the ratio of the two spectra at 10 cm^{-1} the depolarization factor of the first mode is close to $\rho_{dep} = I_{\perp}/I_{\parallel} = 0.75$, as must be the case for a non-resonant non-totally symmetric mode. If we assume our spectra components to have only two different depolarization factors, then the shape of the scattering with depolarization factor different from 0.75 is given by $I_{\parallel} * 0.75 - I_{\perp}$. As a result, two vibrational modes are observed: the first one with a maximum at 10 cm^{-1} (determined from the crossed configuration) and the second one with a broad maximum around 20 cm^{-1} (determined from the calculated spectra).

IV. DISCUSSION

First, we want to see how the free sphere model (A) compares with our experimental results. Table I presents the calculated vibrational energies for a free isotropic sphere of diameter 6.8 nm with the density of silicon and different sound speeds corresponding to important crystal directions in silicon. The first and second [110] lines correspond to transverse phonons polarized along $[\bar{1}10]$ and $[001]$ respectively. Uniformly averaging over all directions, the longitudinal and transverse speeds of sound in silicon are $(9017 \pm 233) \text{ m/s}$ and $(5372 \pm 385) \text{ m/s}$, respectively, where one standard deviation of the variation is indicated. The average rms speed is nearly the same. For comparison, energies were also calculated using these averaged sound speeds. Elastic parameters were taken from¹⁸. As reported by Fujii et al.¹⁶, these frequencies can't explain the lowest band position. Nevertheless,

TABLE I: Energy (ν in cm^{-1}) of the fundamental spheroidal (SPH) and torsional (TOR) vibration mode of a 6.8 nm diameter free silicon nanoparticle for different sound speeds using methods (A) and (C). $Im(\nu)=0$.

Calculation method	Speed of sound	SPH			TOR	
		$l=0$	$l=1$	$l=2$	$l=1$	$l=2$
(A)	[100]	28.3	26.4	23.6	52.5	22.8
(A)	[111]	38.7	28.0	21.1	45.8	19.9
(A)	[110]	38.8	26.0	19.3	42.0	18.3
(A)	[110]	33.8	29.1	23.7	52.5	22.8
(A)	average	35.4	28.2	22.0	48.3	21.0
(C)	anisotropic	34.9	27.0	19.4	50.4	19.4

we will use these results to choose the isotropic parameters which best describe the calculated anisotropic energies. From Table I, the closest agreement with the exact anisotropic calculation (C) is obtained when method (A) uses the averaged sound speeds.

We applied method (B), with averaged sound speeds, to silicon nanoparticles embedded in silica glass. Elastic parameters for silica were taken from¹² and¹⁹. Results are presented in Table II. Results using method (A) (free sphere) are also shown, for which case there is no damping. Modes can be spheroidal (SPH) or torsional (TOR). l is the orbital quantum number and n is the index of the solution. Blank spaces in the free case indicate that there is no equivalent to the corresponding embedded mode.

The silica matrix has three effects: it shifts energies ($Re(\nu)$), it creates damping ($Im(\nu)$) and it also introduces new modes. One of these new modes is (TOR, $l=1,n=0$). In the absence of the matrix this would correspond to rigid rotation. The matrix imposes a restoring force changing the rotation into a libration (rigid rotational oscillation). Other new modes have more complicated origins. Considering modes existing in the free case, the more their energies are shifted, the greater the damping. This is consistent with a stronger contribution of the matrix. The damping values given in Table II correspond to the Raman homogeneous half width at half maximum. The observed Raman linewidth should be greater mainly because of the nanoparticle size distribution inside our samples.

For comparison purposes, calculated energies and damping of vibrations of a 6.8 nm diameter spherical cavity in silica as well as around an infinitely hard, heavy sphere are presented in Table III. In particular, the lowest spheroidal modes in Table II correspond approximately to modes around a rigid, heavy sphere.

From Table II, two modes are good candidates for the lowest Raman peak: (SPH, $l=1,n=1$) and (TOR, $l=1,n=0$). But SPH modes with odd l and TOR modes with even l have odd parity and should be Raman inactive²⁰. The calculated damping for (TOR, $l=1,n=0$) is higher than the Raman peak HWHM. Moreover, size and shape distributions¹⁷ and temperature broadening also increase the Raman linewidth. A possible explana-

TABLE II: Energy ($Re(\nu)$ in cm^{-1}) for free (method (A)) and silica embedded (method (B)) 6.8 nm diameter silicon nanoparticles for various modes. In the embedded case damping ($Im(\nu)$ in cm^{-1}) is the half width at half maximum.

mode	l	n	free (A)	embedded (B)	
			energy	energy	damping
SPH	0	0	35.4	38.3	13.9
		1	85.1	85.5	10.9
		2	130.5	130.8	10.5
	1	0		6.3	9.9
		1		9.3	16.2
		2	28.2	32.7	11.4
2	0		18.8	18.2	
	1	22.0	22.5	10.1	
	2	40.2	46.4	14.0	
TOR	1	0		11.8	11.0
		1	48.3	48.4	6.8
		2	76.2	76.3	6.7
	2	0		6.5	12.2
		1	21.0	26.1	13.7
		2	59.7	59.9	7.3

TABLE III: Energy and damping of a silica matrix surrounding a 6.8 nm diameter spherical cavity and an infinitely rigid and heavy sphere. Only even parity modes are shown.

mode	l	n	cavity		rigid heavy sphere	
			energy	damping	energy	damping
SPH	0	0	9.1	7.4		
		2	6.1	4.6	15.2	14.5
	1	1	7.8	20.3		
		2	23.3	11.1		
TOR	1	0	5.1	8.8		

tion is that in our model, the nanoparticle-matrix contact is perfect and therefore more energy is radiated into the matrix than in our sample.

The second mode is in agreement with the calculated (SPH, $l=2, n=0, 1$) modes. Following²¹, we assume the de-

polarization factor of this peak to be 1/3. Therefore, we are able to fully decompose each spectra. The decomposition for the parallel configuration is shown in Fig. 1.

V. CONCLUSION

The special demands of silicon nanoparticles embedded in silica require consideration of mode broadening by the matrix, mode shifting by the matrix, new modes created by the matrix and the anisotropy of the silicon. A strong candidate as the dominant feature of the Raman spectra is the libration mode (TOR, $l=1, n=0$) which would be Raman inactive without either anisotropy or nonspherical shape²⁰.

The approach we are using can easily be extended to handle other features of realistic nanoparticles, such as non-spherical shape, surface relaxation and details of the nanoparticle-matrix interface. The extension to inhomogeneous onion-like particles where the parameters have radial dependence can also be made.

Exact incorporation of anisotropy is not difficult, but relatively accurate estimates of frequency are possible using an isotropic model of the elasticity as long as direction averaged speeds of sound are used. This works best for modes with $l \leq 1$, since they are at most three-fold degenerate with isotropy and are not split by cubic crystalline anisotropy.

For an isotropic material, the $l=2$ spheroidal and torsional modes are 5-fold degenerate. This degeneracy is broken by the anisotropy, into what MD simulations suggest is a doublet.

Overall, this study has provided a clearer basis for interpreting Raman experiments where the acoustic impedance of the nanoparticle is close to that of the matrix. Crystal elasticity is anisotropic in any case. However, without theoretical calculations of the absolute cross sections of Raman scattering it is possible only to make tentative identification of the vibrational modes that appear in the low frequency Raman spectrum.

* Electronic address: Lucien.Saviot@u-bourgogne.fr

† Electronic address: dmurray@ouc.bc.ca

¹ H. Lamb, Proc. London Math. Soc. **13**, 187 (1882).

² Y. Sato and T. Usami, Geophys. Mag. **31**, 15 (1962).

³ J. G. McDaniel and R. G. Holt, Phys. Rev. E Rapid Comm **61**, R2204 (2000).

⁴ F. Mitri, private communication (2003).

⁵ W. Q. Chen, J. B. Cai, G. R. Ye, and H. J. Ding, ASME J. Appl. Mech. **67**, 422 (2000).

⁶ H. Portalès, L. Saviot, E. Duval, M. Gaudry, E. Cottancin, M. Pellarin, J. Lermé, and M. Broyer, Phys. Rev. B **65**, 165422 (2002).

⁷ W. M. Visscher, A. Migliori, T. M. Bell, and R. A. Reinert, J. Acoust. Soc. Am. **90**, 2154 (1991).

⁸ E. Duval, A. Boukenter, and B. Champagnon, Phys. Rev.

Lett **56**, 2052 (1986).

⁹ C. Voisin, D. Christofilos, N. D. Fatti, and F. Vallée, Physica B **316-317**, 89 (2002).

¹⁰ V. A. Dubrovskiy and V. Morozhnik, Earth Physics **17**, 494 (1981).

¹¹ A. Tamura, K. Higeta, and T. Ichinokawa, J. Phys. C: Solid State Phys. **15**, 4975 (1982).

¹² N. N. Ovsiyuk and V. N. Novikov, Phys. Rev. B **53**, 3113 (1996).

¹³ P. Verma, W. Cordts, G. Irmer, and J. Monecke, Phys. Rev. B **60**, 5778 (1999).

¹⁴ A. C. Eringen and E. S. Suhubi (Academic, New York, 1975), vol. II, pp. 804–833.

¹⁵ F. H. Stillinger and T. A. Weber, Phys. Rev. B **31**, 5262 (1985).

- ¹⁶ M. Fujii, Y. Kanzawa, S. Hayashi, and K. Yamamoto, Phys. Rev. B **54**, 8373 (1996).
- ¹⁷ M. Pauthe, E. Bernstein, J. Dumas, L. Saviot, A. Pradel, and M. Ribes, J. Mater. Chem. **9**, 187 (1999).
- ¹⁸ J. J. Hall, Phys. Rev. **161**, 756 (1967).
- ¹⁹ A. P. Sokolov, A. Kisliuk, M. Soltwisch, and D. Quitmann, Phys. Rev. Lett **69**, 1540 (1992).
- ²⁰ E. Duval, Phys. Rev. B **46**, 5795 (1992).
- ²¹ M. Montagna and R. Dusi, Phys. Rev. B **52**, 10080 (1995).
- ²² Programs are available upon request.
- ²³ see^{6,12,13,16} and references therein.